

Limitations for divertor heat flux calculations of fast events in tokamaks

A. Herrmann, ASDEX Upgrade team

Max-Planck-Institut für Plasmaphysik, EURATOM-IPP Association

Garching and Greifswald, Germany

Introduction

The investigation and optimisation of discharge scenarios with good energy confinement, high density and temperature is a main topic in the research programme of ASDEX Upgrade and other tokamaks. This high confinement (H-mode) regime is envisaged as operation regime for ITER also. The H-mode regime is an operating regime with about 20–30% of the power crossing the separatrix transported not continuously but burst like by edge localised modes (ELMs). The ELM frequency is decreasing and the ELM strength (fraction of energy loss per ELM) is increasing with energy confinement time in present machines, so that the handling of the ELM heat flux into the divertor seems to become an essential problem for ITER. The maximum heat flux is a criterion to decide whether or not a divertor material can withstand the ELMs. This figure is either derived by Langmuir probes or thermography. Both methods have limitations especially for short time events. In the first part of this paper limits of heat flux calculation based on thermographic measurements will be discussed and it will be pointed out that the energy deposited during ELMs is a figure which is robust with respect to changes of the model assumptions. The contribution of radiation cooling and bremsstrahlung as error sources are discussed in the second part.

Heat flux calculation with the THEODOR code

The divertor surface temperature in ASDEX Upgrade is monitored with a high time and spatial resolution IR-line-camera. The temporal resolution of 130 μ s/line allows the detection of single ELMs lasting about 0.5 ms. The measured time evolution of the surface temperature is the input for a numerical 2D heat flux calculation taking into account the temperature dependent material parameters (THEODOR Code). The calculation grid is fitted to the DIV-I situation characterised by flat rectangular carbon tiles made from fine grain graphite (EK 98). The line of view of the IR camera was positioned toroidally in the middle of the tile. This ensures a toroidally symmetric situation so that heat fluxes in the toroidal direction are compensated and the 2D geometry of the model for heat flux calculation holds. The heat conductivity and diffusivity of the fine grain graphite was measured temperature dependent for all three orientations of the graphite [1]. The data of the CFC material and the fine grain graphite used for DIV-II and DIV-IIb, respectively, were measured during manufacturing and with a laser flash method at the IPP-Garching [2]. The geometry and the edge conditions used for the heat flux calculations are shown in Fig. 1. The IR camera was thoroughly calibrated versus a black body radiator. The spectral emissivity of the used carbon was measured in the laboratory by comparing it with black body emission.

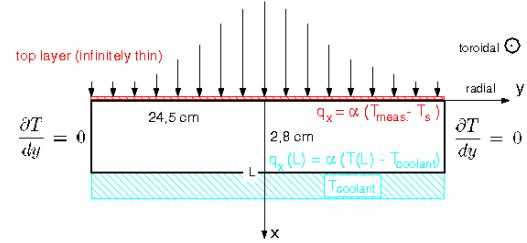


Figure 1. Model used for 2D heat flux calculation in THEODOR

This ensures a toroidally symmetric situation so that heat fluxes in the toroidal direction are compensated and the 2D geometry of the model for heat flux calculation holds. The heat conductivity and diffusivity of the fine grain graphite was measured temperature dependent for all three orientations of the graphite [1]. The data of the CFC material and the fine grain graphite used for DIV-II and DIV-IIb, respectively, were measured during manufacturing and with a laser flash method at the IPP-Garching [2]. The geometry and the edge conditions used for the heat flux calculations are shown in Fig. 1. The IR camera was thoroughly calibrated versus a black body radiator. The spectral emissivity of the used carbon was measured in the laboratory by comparing it with black body emission.

First heat flux calculations for elmy H-mode discharges result in negative heat flux spikes following a heat flux burst (ELM). The duration was comparable to the duration of the burst itself (Fig. 2, blue curve). But, the energy and power balance for these discharges was equated [3]. Such a behaviour is also reported from recent JET IR-measurements [4].

A negative heat flux would mean an active cooling of the surface. This is physical unrealistic for the divertor conditions (see below). A negative heat flux is also expected if the heat flux calculated for previous time values is too high, simulating a too high energy deposition. This overestimated deposition is accompanied by a too high temperature inside the bulk material. The surface temperature decays due to the heat diffusion into the bulk after switching off the heat load. The measured decay is to fast for a zero heat flux and must be compensated by a negative flux because the expected temperature value inside the bulk is higher than the real temperature.

This ‘memory’ is an essential feature of heat flux calculations. On one side it requires to measure the complete temperature evolution starting at a known initial distribution in the bulk. On the other side it is a proof of heat flux calculation in the past. This can be shown for the 1D solution of heat conduction in a semi-infinite target. The evolution of the surface temperature with constant heat flux, q_s , is [5]:

$$T_s = \frac{2}{\sqrt{\pi}} \frac{q_s}{\sqrt{\lambda \rho c}} \sqrt{t} \quad (\text{Eq. 1})$$

and the temperature decay after switching off this heat flux of the duration, τ , is:

$$T_s(t) = T_{\max} \left(\sqrt{1 + \frac{t}{\tau}} - \sqrt{\frac{t}{\tau}} \right) \quad (\text{Eq. 2})$$

with

$$T_{\max} = \frac{2}{\sqrt{\pi}} \frac{q_s}{\sqrt{\lambda \rho c}} \sqrt{\tau} .$$

For $t \leq \tau$ Eq. 2 may be approximated by :

$$T_s(t) = T_{\max} \exp \left(-\sqrt{\frac{t}{\tau}} \right).$$

Plotting the temperature decay versus time allows to derive the height and the duration of the heat puls without any knowledge about the history (Eq. 1).

There are different explanations which may cause negative heat flux values, e.g. (i) in front of the target exists a photon source (molecular radiation, bremsstrahlung) which becomes stronger with ELMs; (ii) there are power loss processes which are not switched off together with the heat flux from the plasma (Planck radiation, evaporation cooling); (iii) the surface is damaged due to plasma wall interaction. This damage should result in a lower thermal transport properties.

Explanation (i) would lead to an unbalanced power and energy balance on longer time scales which is not found. The mentioned loss channels mentioned in (ii) are negligible as discussed below. Surface modifications (iii) due to hydrogen or impurity implantation in

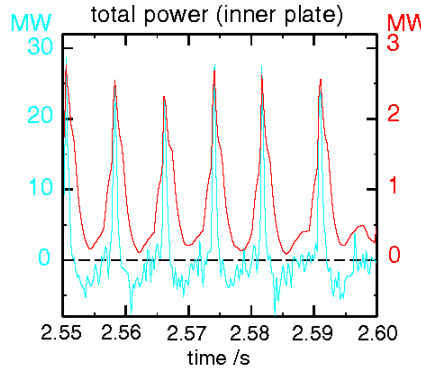


Figure 2. calculated target heat flux (THEODOR) with (red) and without (blue) heat transmission edge condition.

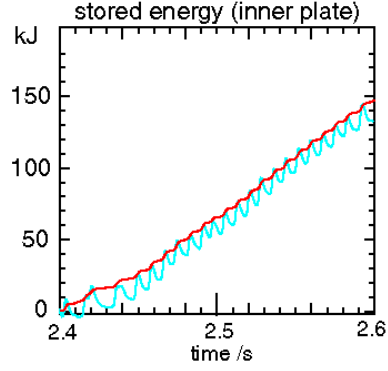


Figure 3. Stored energy calculated from data of fig. 2

erosion dominated regions or due to carbon deposition is observed experimentally. Both effects result in a decrease of the heat conductivity in a thin layer at the top of the surface.

The stationary temperature difference across a layer of thickness, d , is $\Delta T = q_s \frac{d}{\lambda_{layer}}$. This is equivalent to a heat transmission edge condition, $q_s = \alpha(T_{meas} - T_{bulk})$, as used in THEODOR, with a heat transmission coefficient $\alpha = \frac{\lambda_{layer}}{d}$. The criteria to find a heat transmission coefficient was to omit negative heat fluxes. A value of about $\alpha = 100 \frac{kW}{m^2 K}$ was found to be a good compromise between minimising negative heat fluxes and smoothing the burst. Figure 2 shows the heat peaks calculated with and without the edge conditions and the corresponding energy accumulated at the target plate (Fig. 3). It is obvious that the deposited energy in contrast to the power load, did not depend on the value for the heat transmission coefficient. The reason for this is the ‘memory’ effect mentioned above.

In addition to the experimental results shown in Fig. 2 and 3 the top layer effect was simulated using the temperature evolution for the 1D problem (Equ. 1, 2) together with the temperature increase due to the layer itself, $T_{measured} = \frac{q_s}{\alpha} + T_S$, as input for the THEODOR code. A stationary heat flux of $q_s = 5 \frac{MW}{m^2}$, and temperature independent CFC material data are used. ELMs are implemented by adding heat pulses of 0.9 ms duration with a maximum heat flux $q_s = 50 \frac{MW}{m^2}$ at a frequency of 100 Hz. Two values for the heat transmission coefficient were used, $\alpha_1 = 140 \frac{kW}{m^2 K}$ for the layer, and $\alpha_2 = 140 \times 10^{10} \frac{kW}{m^2 K}$, neglecting a layer. Each temperature evolution was the input for heat flux calculation with

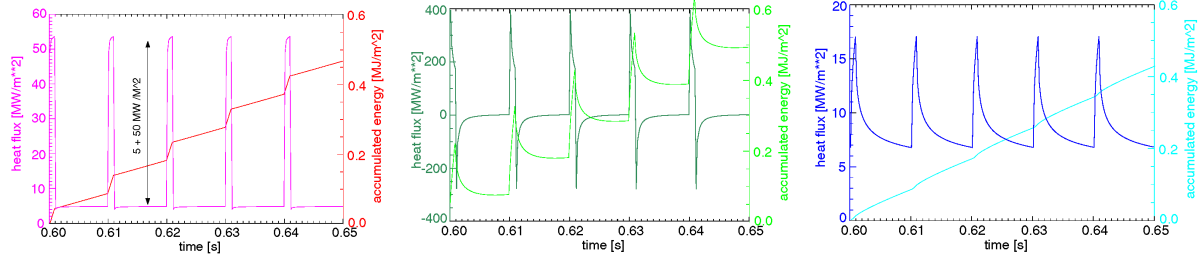


Figure 4. Calculated heat flux with equal α for temperature and heat flux calculation.

Figure 5. Calculated heat flux with α_1 in temperature and α_2 in heat flux calculation.

Figure 6. Calculated heat flux with α_2 in temperature and α_1 in heat flux calculation.

THEODOR, using both values for α . The results are shown in Fig. 4, 5, and 6. Fig. 4 is a proof of the method. The top layer is not considered in the calculation for Fig. 5 and the maximum heat fluxes is overestimated by a factor of 10. If the top layer is not included in the temperature input (Fig. 6) but considered in the heat flux calculation the resulting bursts are smoothed and the maximum heat flux is reduced by a factor of 3. The difference in the accumulated energy for the discussed calculations is $\pm 10\%$.

Radiation cooling and Bremsstrahlung

The measured surface temperature is caused by a net heat flux consisting of heating and cooling contributions. In the context of this paper the strength of cooling contributions,

especially radiation cooling, should be discussed. Radiation losses of a surface at temperature, T_s , with an emissivity, α , are given by:

$$q_{rad} = \epsilon\sigma(T_s^4 - T_u^4)$$

This value has to be compared to the heat flux causing the temperature increase during the time interval, Δt , calculated from Eq. 1. This ratio of radiation loss to net heat flux is shown in Fig. 7. Heat flux values typical for ASDEX Upgrade discharges are marked. They are well below the 1% limit which will be crossed only for long lasting shots with moderate heat flux. Evaporation cooling reaches the same order as radiation losses at a temperatures of about 3000K so that it is much lower than the radiative contribution for the situation considered here [6,7].

Bremsstrahlung and possibly recombination or molecular radiation emits Photons in the detection wavelength range of the detector and is interpreted as temperature signal during the heat flux calculation. Switching off this radiation source results immediately into a decrease of the calculated temperature and may cause the calculation of a negative heat flux. This effect is estimated in [8]. It was found that the bremsstrahlungs contribution in a high density discharge below the density limit is comparable to a temperature increase of $\Delta T=10$ K at a target temperature of 340 K. This contribution is negligible at higher target temperatures because of the exponential increase of the photon flux with surface temperature.

Conclusions

The heat transfer edge condition used in the heat flux calculation with THEODOR allows a robust calculation of the energy deposited during short time events like ELMs due to the ‘memory’ of the bulk temperature. The maximum heat flux is dramatically changed with changing surface conditions and can not be used without carefully checking its temporal evolution. Radiation cooling and evaporation may be neglected for short heat flux pulses in ASDEX Upgrade. Parasitic photon radiation due to bremsstrahlung is negligible for surface temperatures a few ten degrees above room temperature.

References

- [1] W. Delle, J. Linke, H. Nickel, E. Wallura, JüL-Spez-401, May 1987, ISSN 0343-7639
- [2] Netzschi LFA 927, Stefan Lindig, material science department
- [3] A. Herrmann, W. Junker, K. Günther et al., Plasma Phys. Control. Fusion 37 (1995) 17
- [4] Th. Eich, ‘Analysis of power deposition in JET MKIIGB divertor by IR-thermography’, this conference
- [5] Carslaw and Jaeger, Conduction of heat in solids, Oxford University Press
- [6] V. Phillips, private communication;
- [7] H. Vernickel, J. Nucl. Mater. 111&112(1982)531
- [8] A. Herrmann, ‘Optical surface temperature measurement’, in Diagnostic for Experimental Thermonuclear Fusion Reactors, Edited by P. Stott et al., Plenum Press, New York, 1996, p581

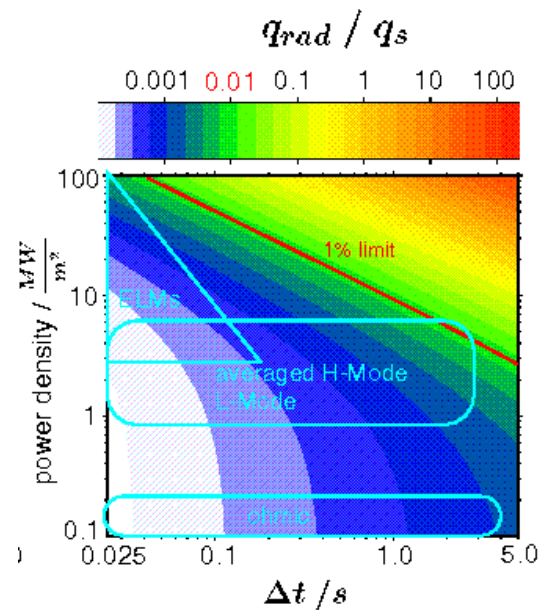


Figure 7. Ratio of radiation loss and net heat flux for heat pulses of the duration Δt